

Hydrogenated carbon structures as directional sub-GeV dark matter detectors

Tomás Arias,¹ Antonino Bellinvia,² Gianluca Cavoto,^{2,3,*} Angelo Esposito,^{2,3,†} Francesco Pandolfi,^{3,‡} Guglielmo Papiri,^{1,§} Antonio D. Polosa,^{2,3,¶} and Tyler Wu¹

¹*Department of Physics, Cornell University, Ithaca, New York 14853, USA*

²*Dipartimento di Fisica, Sapienza Università di Roma, Piazzale Aldo Moro 2, I-00185 Rome, Italy*

³*INFN Sezione di Roma, Piazzale Aldo Moro 2, I-00185 Rome, Italy*

(Dated: February 4, 2026)

We propose hydrogenated carbon structures as targets with a remarkable sensitivity to dark matter–nucleon interactions, in the mass range between the 1 MeV and 100 MeV. The ejection of a proton following the interaction with a dark matter particle is a quasi-elastic process, with an extremely small energy threshold, and a clear experimental signature. The proposed detectors are simple, technologically ready, and inexpensive. Yet, they can be considerably more sensitive than current experiments. They also allow strong directionality, to be used towards efficient background rejection.

I. INTRODUCTION

Despite being one of the most compelling problems in fundamental physics, the search for Weakly Interacting Massive dark matter Particles (WIMPs) has so far only reported null results [e.g., 1–8]. This has fueled several efforts towards finding new ways to probe yet unexplored regions both in mass and couplings, as suggested by a number of theoretical models [e.g., 9–17]. In particular sub-GeV dark matter particles cannot be detected in elastic scatterings with most of the detector targets, because of the large mass mismatch with the recoiling nuclei. Those experiments that are currently looking into the MeV to GeV range, or propose to do so, circumvent this limitation by trying to detect inelastic processes [e.g., 17, 18], such as phonon emission in various materials [e.g., 2, 7, 19–25] or the Migdal effect [e.g., 5, 26–28] which, however, have much smaller rates.

We propose the use of *hydrogenated* carbon structures, such as graphene, graphite or nanotubes (CNTs), to search for dark matter particles interacting with nucleons. Indeed, when a sub-GeV dark matter particle impinges on the proton belonging to one of the hydrogen atoms, it can exchange enough energy to release it via an almost *elastic* process. Once emitted in a vacuum enclosure, the charged proton can be accelerated by an electric field, and eventually be collected. The proposed detector has an extremely low energy threshold: as the typical binding energy of a proton onto a carbon structure is of the order of a few eVs [e.g., 29–31], dark matter particles with masses $m_\chi \sim \mathcal{O}(\text{MeV})$ can eject protons with sizable rates. In the case of vertically aligned CNTs, the expected signal is directional, thus providing a strong handle for background rejection. Graphene and CNTs have been studied both theoretically and experimentally to probe dark matter

electron interactions [32–36], constrain the neutrino mass and hunt the elusive relic neutrinos [e.g., 29, 31, 37].

The technology behind the hydrogenation of carbon structures is well assessed [e.g., 38–42], making it possible to engineer the supporting graphene holder in order to optimize it towards the present proposal. Moreover, the proton binding energy can be varied by manipulating the hydrogenation level and/or the local geometry of the substrate [e.g., 29–31]. Hydrogenated graphene is also stable at room temperature [43], making this detection scheme practically insensitive to thermal effects. This means that it can fit in a relatively small high-vacuum chamber, without the need for expensive infrastructures, such as cryostats. In the proposed detector, the ejected proton emerges from an anode, which is kept at a positive voltage of a few kVs. It can then be easily directed towards a sensor by a suitably shaped electric field. This sensor, having a sensitive area much smaller than the hydrogenated substrate, can be a single channel silicon drift detector (SDD). A SDD can also measure the accelerated proton energy with a resolution sufficient to separate signal from background [44]. (See the Conclusions for a discussion on this.) The hydrogenated carbon structures considered here, as well as the proposed experimental concept, are shown in Figure 1.

We consider a simple benchmark model of spin-independent dark matter–nucleon interactions, and employ Density Functional Theory (DFT) [e.g., 45, 46] to determine the expected rate for the liberation of a proton from the substrate. We do that for both graphene and CNTs. CNTs, in addition to offering substantially more target mass per unit area, are expected to exhibit directional sensitivity. In this case, however, one must also estimate the probability that the proton emitted by the dark matter scattering is transmitted to the exterior of the forest, without being lost or captured by the material itself. We do that with a suitably-designed Monte Carlo simulation. In all these instances, we find that the proposed materials can outperform by orders of magnitude the best current experimental constraints [e.g., 5, 28].

* gianluca.cavoto@roma1.infn.it

† angelo.esposito@uniroma1.it

‡ francesco.pandolfi@roma1.infn.it

§ gp343@cornell.edu

¶ antonio.polosa@roma1.infn.it

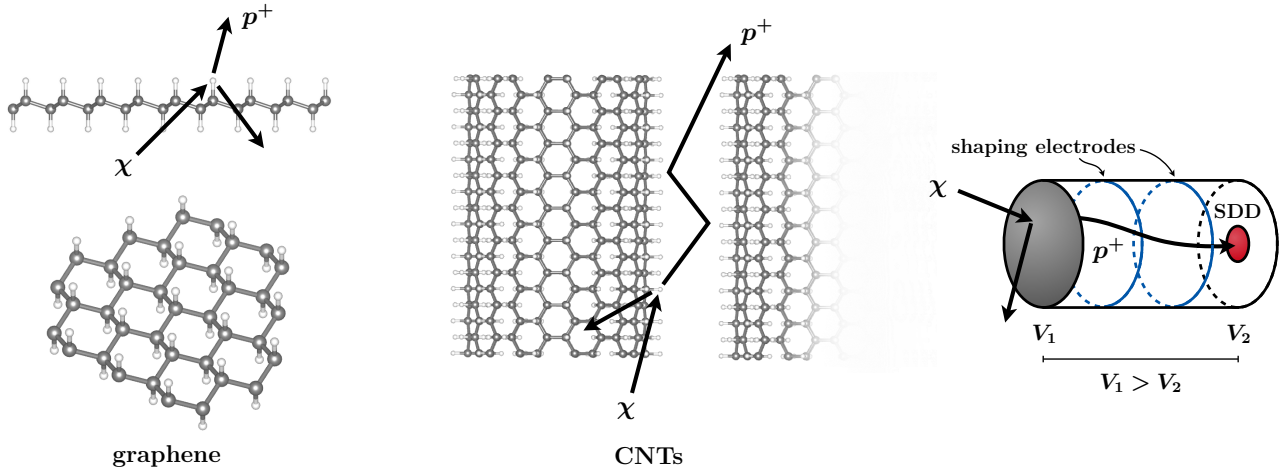


FIG. 1. **Left and central panels:** Schematic representation of the hydrogenated carbon structures at 100% loading, and a pictorial dark matter interaction on a hydrogen nucleus, resulting in the ejection of a proton. Dark and light spheres represent respectively carbon and hydrogen atoms, with the latter being covalently bound to their carbon site. **Right panel:** Detector concept. After its ejection, the proton is accelerated by an electric field, and its trajectory is focused by shaping electrodes, until it is detected by an SSD.

II. THE DARK MATTER–PROTON COLLISION

We consider a benchmark model of fermionic dark matter interacting with protons via a spin-independent interaction mediated by a heavy scalar, $\mathcal{L}_{\text{int}} = g_\chi \phi \bar{\chi} \chi + g_p \phi \bar{p} p$, where we assume $m_\phi \gg m_\chi v_\chi$, with v_χ the typical dark matter velocity. From the quantum-mechanical viewpoint, this is matched to a contact interaction potential,

$$U(\mathbf{x}_\chi, \mathbf{x}_p) = -\frac{g_\chi g_p}{m_\phi^2} \delta(\mathbf{x}_\chi - \mathbf{x}_p). \quad (1)$$

The initial state proton is bound to the carbon structure, and it is thus necessary to account for its wave function and binding energy. Realistic CNTs have a radius of order 10 nm, much larger than the size of a unit cell. Consequently, they can also be approximated as locally flat. We will assume a local coverage of 100%, meaning that all carbon sites surrounding a given hydrogen atom are also occupied, and neighboring hydrogen atoms sit on opposite sides of the graphene layer.¹ This configuration, sometimes dubbed “graphane”, has been discussed in detail in [29, 31] for the case of tritiated graphene. The initial proton wave function is

$$\psi_0(\mathbf{x}_p) = \frac{1}{\pi^{3/4} \lambda_{\parallel} \sqrt{\lambda_{\perp}}} \exp \left(-\frac{x_{p,\parallel}^2}{2\lambda_{\parallel}^2} - \frac{x_{p,\perp}^2}{2\lambda_{\perp}^2} \right), \quad (2)$$

where $x_{p,\parallel}$ and $x_{p,\perp}$ are the directions parallel and perpendicular to the graphene plane, respectively. Upon a rescaling from the tritium to the proton mass, the parallel and

perpendicular spreads are $\lambda_{\parallel} \simeq 0.17 \text{ \AA}$ and $\lambda_{\perp} \simeq 0.11 \text{ \AA}$, while the binding energy is $\varepsilon_0 \simeq -4.5 \text{ eV}$ [31].

In this work, we use graphene as a benchmark two-dimensional material, although large areas might be achieved more easily leveraging the surface of graphite. The 100% loading configuration described above, however, is not realizable on graphite, as the bottom part of the carbon sites are bound to another graphene layer, and the hydrogenation is expected to happen all on the same side. A similar situation happens for CNTs. The 100% loading configuration is only realizable on single-wall CNTs, which can be synthesized in lab [e.g., 47, 48]. For the more common multi-wall CNTs, hydrogenation happens on only the exterior of the tube. Nonetheless, the parameters characterizing the binding of the proton depend on the loading and spatial distribution only by, at most, a factor of order one [29–31]. Our proposal and conclusions are thus unaffected.

For the processes of interest, the final state proton is free. Its wave function, as well as those of the incoming and outgoing dark matter, are then well approximated by plane waves. We normalize them to unity when working at some finite volume, V . The corresponding matrix element then reads,

$$\mathcal{M} \equiv \langle \mathbf{k}', \mathbf{p} | U | \mathbf{k}, \psi_0 \rangle = -\frac{g_\chi g_p}{V^{3/2} m_\phi^2} \hat{\psi}_0(\mathbf{k} - \mathbf{k}' - \mathbf{p}), \quad (3)$$

where \mathbf{k} , \mathbf{k}' , and \mathbf{p} are the momenta of the incoming dark matter, the outgoing one, and the outgoing proton, while $\hat{\psi}_0$ is the Fourier transform of the proton’s initial wave function. Given this, the rate of ejection of a proton by a dark matter is obtained from Fermi’s golden rule:

$$d\Gamma = 2\pi |\mathcal{M}|^2 \delta(\varepsilon_0 + E_k - E_{k'} - E_p) \frac{V d\mathbf{k}'}{(2\pi)^3} \frac{V d\mathbf{p}}{(2\pi)^3}, \quad (4)$$

¹ Note that a *local* coverage of 100% does not necessarily mean that all carbon sites of the *macroscopic* sample are hydrogenated.

where the E 's are kinetic energies, with obvious definitions. Finally, the expected experimental rate is obtained by accounting for the number of available protons, N_H , the mass density of incoming dark matter, ρ_χ , as well as its velocity distribution in the Milky Way halo, $f(v)$. Specifically, it is given by,

$$R(\hat{v}_e) = V N_H \frac{\rho_\chi}{m_\chi} \int d\mathbf{v} f(|\mathbf{v} + \mathbf{v}_e|) \Gamma(\mathbf{v}), \quad (5)$$

where Γ is the total rate obtained by integrating Eq. (4), which depends on the dark matter velocity through its initial momentum. We take the velocity distribution to be a truncated Maxwellian as in the standard halo model, with dispersion $v_0 = 230$ km/s, escape velocity $v_{\text{esc}} = 600$ km/s, and boosted with respect to the Galactic rest frame by the Earth velocity, $v_e = 240$ km/s [49, 50]. We also take the dark matter mass density to be $\rho_\chi = 0.4$ GeV/cm³ [49, 51]. We also anticipated the possible directionality of our signal, through the dependence of the rate on the direction of the Earth's velocity. The direction of the “dark matter wind” is opposite to \hat{v}_e .

III. 2D: GRAPHENE

Eq. (5) provides the ideal rate for the liberation of a proton from the surface of the carbon structure. Yet, not all events are experimentally detectable. A possible obstacle lies in the fact that the proton could be ejected together with one of the electrons which were originally localized in its vicinity. This would produce a neutral hydrogen, which is much harder to detect.

We performed a DFT analysis to estimate the probability that the interaction ejects a naked proton, with no electrons around it. Given our flat graphene with a 100% coverage, we computed the probability that, after the scattering, all electrons end up in the ground state of the new graphene sheet (identical to the initial one, but with one fewer proton). As described in detail in Appendix A, we do that within the sudden approximation for the dark matter–proton interaction. This is valid for all masses of interest, except for those right around the MeV, where corrections are expected. We conservatively find that the probability of ejecting a naked proton is,

$$P_{\text{proton}} \gtrsim 72\%. \quad (6)$$

As far as graphene is concerned, after the proton is liberated without electrons bound to it, it is accelerated with a suitable electric field, and eventually collected by the detector—see again Figure 1. The final rate is then,

$$R_{\text{graphene}}(\hat{v}_e) = R(\hat{v}_e) P_{\text{proton}}. \quad (7)$$

We report the corresponding projections in Figure 2, computed in a configuration with the dark matter wind orthogonal to the graphene layer. The strength of the dark matter–proton interaction is represented with a reference cross section, $\bar{\sigma}_p \equiv g_\chi^2 g_p^2 \mu_{\chi p}^2 / (\pi m_\phi^4)$, where $\mu_{\chi p}$ is

the dark matter–proton reduced mass. We show two instances: a conservative one considering a graphene sheet of area 100 cm², and a more ambitious one with an area of 1 m². Assuming that our graphene sample is globally fully hydrogenated, these correspond respectively to a target mass of $M_H \simeq 0.66$ and 66 μg . As one can see, already with this simple setup, the expected sensitivity is considerably better than the current experimental bounds. The minimal mass that can be probed by this detector is dictated by the initial proton binding energy, which must be overcome by the dark matter kinetic energy. This leads to $m_\chi^{\min} = 2|\varepsilon_0|/(v_{\text{esc}} + v_e)^2 \simeq 1.1$ MeV.

IV. 3D: NANOTUBES

Along similar lines, one can consider hydrogenated CNTs. This allows for a three-dimensional target, thus gaining considerably more target mass if compared with a graphene/graphite setup with equal surface area. Arrays of aligned CNTs have already been considered as a possible target for direct dark matter detection. In particular, extensive work has been done in trying to employ them to hunt for possible dark matter–electron interactions [32–36]. As far as the dark matter–nucleon coupling is concerned, they were originally considered to look for processes where the dark matter ejects a carbon nucleus [52, 53]. Owing to the large carbon mass, this allowed to probe masses no lighter than a few GeVs.

In our case, instead, the target is a proton. Once emitted, the proton must travel to the outside of the array of CNTs, to be eventually detected. Before doing that, however, the vast majority of the protons scatter multiple times on the surface of the CNTs. It is therefore necessary to understand the result of these interactions: whether they scatter off elastically, inelastically, or if they get captured and lost.

A number of recent experimental results have investigated the behavior of protons impinging on the surface of graphene which, we recall, is locally very similar to single-wall CNTs. Among other things, these data show that (a) graphene is somewhat permeable to protons with kinetic energies above about 1 eV [e.g., 54–58], and (b) proton absorption on the layer is strongly suppressed when their kinetic energy is below about 0.2 eV [59].² Since the degree of permeability is hard to quantify at this stage, we adopt a conservative assumption: any proton with energy orthogonal to the surface of the CNT exceeding

² This behavior differs from that of other ions which, instead, are blocked and absorbed by single layer graphene [e.g., 54–59]. We also point out that early calculations suggested that protons are neutralized by the interaction with solid surfaces [e.g., 60–63]. Such results seem to be at odds with the above mentioned experiments. Nonetheless, we notice that they are obtained for proton kinetic energies larger than 100 eV, far from the regime discussed here.

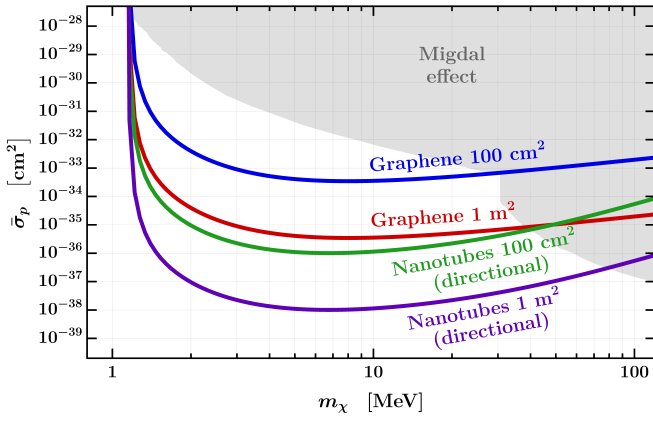


FIG. 2. Projected reach at 90% C.L., assuming no background. The target mass corresponding to graphene of area 100 cm^2 and 1 m^2 is, respectively, $M_H = 0.66$ and $66 \mu\text{g}$. For CNTs of area 100 cm^2 and 1 m^2 it is, instead, $M_H = 0.84$ and 84 mg . The gray shaded areas correspond to currently excluded region, as obtained using the Migdal effect, whose leading bounds are set by SENSEI [5] and PandaX-4T [28]. The reference cross section is defined as $\bar{\sigma}_p \equiv g_\chi^2 g_p^2 \mu_{\chi p}^2 / (\pi m_\phi^4)$.

$E_\perp > 0.2 \text{ eV}$ undergoes some inelastic processes, loses energy, and is eventually captured. Only protons with $E_\perp < 0.2 \text{ eV}$ scatter elastically off the walls of the CNTs. With this at hand, there are three possible fates for one of the protons ejected by the dark matter:

- If its energy is $E_\perp > 0.2 \text{ eV}$, it gets captured after interacting with the CNT wall.
- If its energy is $E_\perp < 0.2 \text{ eV}$, but it leaves the array from either the bottom or from the sides, preventing its collection and observation.
- Its energy is $E_\perp < 0.2 \text{ eV}$, and it manages to leave the array from the top.

Among these possibilities, only the last one is favorable to our setup. We indicate its probability as $P_{\text{exit}}(\hat{\mathbf{v}}_e)$, anticipating the fact that, as shown below, this depends on the direction of the dark matter wind.

To determine the fraction of protons that manage to leave the CNTs forest from the top, we run a suitably designed Monte Carlo simulation, whose details are reported in Appendix C. First of all, given the size of the array considered in our simulation, lateral exits happen only for a small fraction of events. This fraction becomes even smaller for arrays of larger area, as it becomes much more likely for a proton to reach the top before reaching the sides. The results for the probability that a proton escapes from the top are reported in Figure 3. As one can see, this probability decreases strongly with increasing dark matter masses. Indeed, higher masses imply a much larger chance for the outgoing proton to have $E_\perp > 0.2 \text{ eV}$, and thus fall among those events that we consider as lost. From the large difference between the

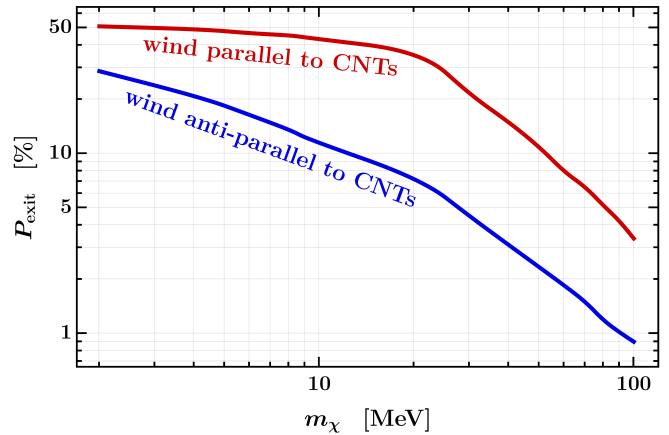


FIG. 3. Probability for a proton to leave from the top side of the array of CNTs as a function of the dark matter mass, computed for a dark matter wind parallel (red curve) and anti-parallel (blue curve) to the orientation of the CNTs.

two curves we also deduce that we expect order one modulations, when the direction of the dark matter wind with respect to the orientation of CNTs changes. This can be used as a powerful leverage to discriminate the signal from the (isotropic) background. The modulation decreases for masses $m_\chi \lesssim 10 \text{ MeV}$. This is indeed the regime where the typical dark matter momentum becomes smaller than the inverse spread of the initial proton wave function, $m_\chi v_\chi \lesssim 1/\lambda_{\parallel}, 1/\lambda_\perp$ —see Eq. (2). Momentum conservation is then maximally broken by the wave function, and the final state proton retains less information about the direction of the incoming dark matter.

In light of all this, the expected event rate for an array of CNTs is given by,

$$R_{\text{CNT}}(\hat{\mathbf{v}}_e) = R(\hat{\mathbf{v}}_e) P_{\text{proton}} P_{\text{exit}}(\hat{\mathbf{v}}_e), \quad (8)$$

where P_{proton} is the probability reported in Eq. (6). The corresponding projected sensitivity is again shown in Figure 2. Specifically, we assume for the CNTs to have a diameter of 10 nm , a distance of 50 nm between their centers, and a height of $100 \mu\text{m}$ [64]. For arrays with area 100 cm^2 and 1 m^2 the corresponding target mass is $M_H = 0.84$ and 84 mg , respectively.

V. CONCLUSION

We proposed the use of hydrogenated graphene, possibly graphite, and carbon nanotubes as targets to probe dark matter–nucleon interactions, for masses as light as $m_\chi \sim \mathcal{O}(\text{MeV})$. Thanks to the weak carbon–hydrogen bond, and the quasi-elastic nature of the interactions, this setup is characterized by a small energy threshold, and a detection scheme based on these materials is expected to be orders of magnitude more sensitive than current experiments.

The setup is expected to be inexpensive and easy to operate. Hydrogenated graphene and graphite are simple

systems, with well understood properties, thus allowing to envision the realization of this proposal in a short time scale and with a reasonable opportunity to scale up the instrumented target mass. Moreover, CNTs provide substantially more target mass than an equivalent area of graphene/graphite. They are also expected to provide a strongly directional signal, offering a key tool towards background rejection. Nonetheless, they require better understanding, especially regarding the capture probability of protons scattering off their walls.

Dark matter detectors usually require good shielding against environmental radioactivity and cosmic rays, and to be fabricated with weakly radioactive materials. For instance, gamma rays can interact with the carbon atoms of the substrate and generate background Compton electrons reaching the SDD, and mimicking a dark matter signal. Compton electrons, in fact, can have energies as large at 100 keV, and are therefore not stopped by the applied electric field. Nonetheless, we calculated that, for the 100 cm^2 hydrogenated graphene target, it is sufficient to keep the gamma ray flux below a few Hz to have negligible background events in one year of exposure. A further background suppression technique might be based on the use of a localized magnetic field to deflect electrons.

This work suggests a number of further theoretical and experimental investigations. A more accurate theoretical characterization of the materials will come, together with the study of different dark matter–proton couplings, to present a comprehensive picture of the possible reach of the proposed experiment. From the experimental viewpoint, the proposed mechanism of proton ejection can be validated by mimicking the dark matter particles with epithermal neutrons, with energies in the eV range.

ACKNOWLEDGMENTS

We are grateful to Michele Tarquini for collaboration at the early stages of this project. T. Wu was supported by the US National Science Foundation under award PHY-1549132, the Center for Bright Beams.

Appendix A: Proton’s initial ejection probability

In principle, the final state of the initial dark matter scattering can be complicated: when a proton is ejected from the hydrogenated carbon structure, the electrons in the lattice can be promoted to excited lattice states, they can be ionized and freed from the lattice, or they can be ejected as bounded to the outgoing proton. In this appendix we use DFT to estimate the probability for the final state particle to be a naked proton, without electrons bound to it.

As far as the lattice structure is concerned, we consider a graphene layer with a hydrogen loading of 100%. This corresponds to a configuration where each hydrogen is bound to a carbon site, on alternating sides of the

graphene sheet. Due to their large radius, this provides a good description of realistic carbon nanotubes as well. The nanotubes we consider here, in fact, have a typical radius of the order of tens of micrometers, which is much larger than the size of the graphene unit cell.

We start by using DFT to compute the initial electronic state. We initialize our graphene supercell geometry and place hydrogen atoms regularly on the sheet until we reach the desired hydrogen coverage. Then, we allow the lattice to relax to their equilibrium positions, so that the entire electrons–nuclei system is in its ground state. Using the single-particle wave functions from Kohn–Sham DFT [e.g., 45, 65], we can construct the effective non-interacting electronic ground state as a Slater determinant for the supercell geometry, which we denote as $\Psi_0(\mathbf{x}_1, \dots, \mathbf{x}_N)$, where \mathbf{x}_i are the coordinates of the electrons. We consider this to be the electronic initial state.

To simplify the calculation, we only compute the probability for the event where, after the proton has been ejected, all the electrons remain bound to the lattice, in the original electronic ground state. This is only one of many possible final states. Indeed, as long as the proton is ejected naked, the electrons could end up in any possible excited state of the graphene system, without affecting our detection strategy. The probability computed here, therefore, provides a safe lower bound on the total detection rate achieved in a realistic experiment.

Following the so-called sudden approximation, and the approach developed for the determination of the Migdal effect rate [66], the probability that all electrons remain bound to the graphene sheet after a dark matter–proton scattering event is essentially given by the overlap between the initial ground state total electronic wave function (when the lattice is at equilibrium structure) and the final total electronic wave function when the lattice is modified by removing one proton from its structure.

To be more precise there are three different time scales in this process. The shortest time scale is the one associated to the dark matter–proton interaction. This can be estimated as the time it takes for the dark matter wave function to separate from that of the proton,

$$\tau_\chi \sim \lambda_\chi / v_\chi = \frac{1}{m_\chi v_\chi^2} \lesssim 10^{-15} \text{ s}, \quad (\text{A1})$$

where λ_χ is the dark matter de Broglie wavelength, and we used the fact that we are interested in masses $m_\chi \gtrsim 1 \text{ MeV}$. For masses larger than this, the typical scattering time, τ_χ , become smaller than 10^{-15} s . The time scale associated to the electronic response is, instead, roughly given by,

$$\tau_e \sim 1/\varepsilon_e \sim 10^{-15} \text{ s}, \quad (\text{A2})$$

where ε_e is the electrons’ characteristic energy. This can be take to be of the order of the work function of the hydrogenated graphene system, that is the energy to remove one electron from the system, $\varepsilon_e \simeq 5 \text{ eV}$. Thus, for all masses of interest, the scattering process happens faster

than the electronic response, thus justifying the use of the sudden approximation—modulo possible corrections for masses close to the MeV.

In addition, the characteristic time of the electron response is much shorter than the time scale of the nuclear degrees of freedom of the lattice, τ_L . This guarantees the applicability of the Born–Oppenheimer approximation which is at the basis of standard DFT methods.

To compute the final electronic state, we remove one proton from the sheet without, however, removing its electron. The total number of electrons is thus unchanged. Given the separation of scales discussed above, we do not allow for the lattice to relax, as the electronic degrees of freedom respond much more quickly. We then solve for the new electronic ground state, the one obtained from a lattice with one fewer proton. The corresponding wave function is again obtained as a Slater determinant, which we denote as $\Psi'_0(\mathbf{x}_1, \dots, \mathbf{x}_N)$. The probability of ending up in the new ground state, as determined within the sudden approximations, is then simply,

$$P_{\text{ground} \rightarrow \text{ground}'} = |\langle \Psi_0 | \Psi'_0 \rangle|^2 \simeq 72\%. \quad (\text{A3})$$

As discussed before, this represent a conservative lower bound to the actual probability of emission of a naked proton.

For this calculation, we simulated a supercell geometry corresponding to a finite hydrogenated graphene flake, finding a fast numerical convergence in the calculation up to the size of 7×7 unit cells. Additional details on the DFT computation can be found in the next appendix.

Appendix B: Computational details

For the DFT calculations, we used JDFTx, an open-source DFT software, for the Kohn–Sham eigenstates and energies [67]. In the calculations, we use the Perdew–Burke–Ernzerhof generalized-gradient (gga-PBE) functional, along with the SG15 norm-conserving pseudopotentials [68, 69]. The plane wave cutoff we used was 30 Hartrees. To limit periodic image interactions for planar and isolated geometries, we used Coulomb truncation [70].

For the calculation of the initial proton ejection probability, we used two hydrogenated graphene flakes consisting of N -by- N primitive cells where the second flake has a hydrogen atom missing near the center. Letting $N = 4, 5, 6, 7$, we compute the probabilities and extrapolate the converged value as $N \rightarrow \infty$. To limit edge effects, we decorate the boundary of the flake with hydrogen atoms at appropriate carbon–hydrogen bonding sites. The length of the box in the normal direction is set to 30 Bohrs. Since the system is meant to be isolated in vacuum, we used Gamma-point-only Brillouin-zone sampling, i.e. we retained only Bloch states with zero crystal momentum; this one-k-point approximation is commonly used for large supercells, where the Brillouin zone becomes correspondingly small [71]. The states are

then indexed by a single integer. Using Slater determinant states for the electron ground states, the probability in Eq. (A3) is obtained from,

$$\langle \Psi_0 | \Psi'_0 \rangle = \det(\langle \psi'_m | \psi_n \rangle). \quad (\text{B1})$$

Here the determinant is computed of the m and n indices labeling the single-electron states. Moreover, ψ and ψ' are the states computed, respectively, before and after the removal of the proton.

Appendix C: Simulation of the fate of the proton

The trajectory and scattering off the walls of the CNTs are simulated with Monte Carlo methods implemented in **Julia** and **Mathematica**. Specifically, **Julia** models the detector geometry and proton transport in the nanotube forest, while **Mathematica** treats the dark matter–proton interaction and samples the proton’s initial velocity.

We model a detector consisting of a square grid of 10^4 nanotubes per side, $100 \mu\text{m}$ in height, 10 nm in diameter, and with 50 nm spacing between adjacent nanotube centers, making the array area $0.5 \text{ mm} \times 0.5 \text{ mm}$. To speed up the simulation, the full grid is simulated by applying periodic boundary conditions to a single square cell with two nanotubes per side.

The simulation consists in the following main blocks.

1. Random sample of the dark matter velocity. This is done by an accept-reject method, from a distribution given by a truncated Maxwellian following the standard halo model, as described in the main text.
2. Given the dark matter velocity, we extract the momentum of the ejected proton, as dictated by the differential distribution obtained from Eq. (4). Due to bad numerical convergence, for masses $m_\chi > 10 \text{ MeV}$, we approximate the proton wave function as isotropic, $\lambda_{||} = \lambda_\perp$. For large exchanged momenta, anisotropic effects are anyway negligible. The two distributions are the following:

$$\frac{d\Gamma_{\text{isot}}}{d\mathbf{p}} \propto \frac{e^{-\lambda^2(q^2+k'^2)}}{q} \sinh(2\lambda^2 q k'), \quad (\text{C1a})$$

$$\begin{aligned} \frac{d\Gamma_{\text{anisot}}}{d\mathbf{p}} \propto & k' \int_{-1}^1 d\cos\theta I_0(2\lambda_{||}^2 q_{||} k' \sin\theta) \\ & \times e^{-\lambda_{||}^2(q_{||}^2+k'^2 \sin^2\theta)} \\ & \times e^{-\lambda_\perp^2(q_\perp^2+k'^2 \cos^2\theta-2q_\perp k' \cos\theta)}, \end{aligned} \quad (\text{C1b})$$

where, for the isotropic distribution, we took $\lambda \equiv (\lambda_{||} + \lambda_\perp)/2$, and we defined $\mathbf{q} = \mathbf{k} - \mathbf{p}$, with \mathbf{k} and \mathbf{p} the momenta of the incoming dark matter and outgoing proton, respectively. Moreover, q_\perp and $q_{||}$ are the components orthogonal and parallel to the surface of the nanotube, and

m_χ [MeV]	Wind parallel				Wind anti-parallel			
	5	10	50	100	5	10	50	100
$E_\perp > 0.2$ eV events	0.32	0.47	0.87	0.95	0.32	0.47	0.87	0.95
Top exits	0.48	0.40	0.11	0.04	0.18	0.12	0.02	0.01
Bottom exits	0.19	0.12	0.02	0.01	0.49	0.41	0.11	0.04
Lateral exits	< 0.01	< 0.01	< 0.01	< 0.01	< 0.01	< 0.01	< 0.01	< 0.01

TABLE I. Fraction of events falling in the different categories described in the text, evaluated for a total of $N = 10^5$ protons, and for two relative directions of the dark matter wind with respect to the nanotubes: parallel and anti-parallel.

$k' = \sqrt{2m_\chi \left(\varepsilon_0 + \frac{k^2}{2m_\chi} - \frac{p^2}{2m_p} \right)}$, with m_p the proton mass. Finally, I_0 is a modified Bessel function of the first kind.

3. If $E_\perp > 0.2$ eV *or* the proton is emitted downward, the event is discarded. In the first instance it is assumed that it undergoes (yet unknown) energy losses and eventually gets captured. In the second instance, instead, it is guaranteed that it will never leave the forest from the top.
4. If $E_\perp < 0.2$ eV *and* the proton is emitted upward, we have two possible instances:
 - If the proton is ejected toward the interior of the nanotube, it can only undergo multiple scatterings inside the nanotube and eventually leave from the top.
 - If the proton is ejected outside the nanotube, instead, it will scatter off the walls of the other nanotubes in the forest. We then simulate its full trajectory. At each step, we determine which nanotube it interacts with, compute the collision point and extract the vector normal to the surface of the nanotube. After the collision, we flip the sign of the component of the proton's momentum parallel to this vector, while preserving the orthogonal components.

Once the proton trajectory has been simulated there are two possible outcomes: the proton leaves the forest from one of the sides (*lateral exit*), or from the top (*top exit*). Of all these instances, only top exits are favorable under our detection scheme.

We repeat this for $N = 10^5$ protons, and for two possible directions of the nanotubes: parallel and anti-parallel to the dark matter wind. In Table I we report the results of our simulations for a few values of the dark matter mass. Notice that the probability that the initial proton is emitted with $E_\perp < 0.2$ eV and directed upward is nothing but $P_{\text{top}} + P_{\text{lateral}}$, as these are the only two possible outcomes once the proton start moving upward and scatter elastically. Given this, the probability for a proton to leave the array is,

$$P_{\text{exit}} = \frac{1}{2} (P_{\text{top}} + P_{\text{lateral}}) + \frac{1}{2} P_{\text{top}} \simeq P_{\text{top}}. \quad (\text{C2})$$

The first term in the first line is the probability corresponding to the instance where the dark matter hits a proton on the inside of the CNT, while the second term is when it hits a proton on the outside. Finally, in the second line we used $P_{\text{lateral}} \ll P_{\text{top}}$, as shown in Table I

[1] C. Amole *et al.* (PICO), “Dark Matter Search Results from the PICO-60 C₃F₈ Bubble Chamber,” *Phys. Rev. Lett.* **118**, 251301 (2017), [arXiv:1702.07666 \[astro-ph.CO\]](https://arxiv.org/abs/1702.07666).

[2] I. Alkhateb *et al.* (SuperCDMS), “Light Dark Matter Search with a High-Resolution Athermal Phonon Detector Operated Above Ground,” *Phys. Rev. Lett.* **127**, 061801 (2021), [arXiv:2007.14289 \[hep-ex\]](https://arxiv.org/abs/2007.14289).

[3] Yue Meng *et al.* (PandaX-4T), “Dark Matter Search Results from the PandaX-4T Commissioning Run,” *Phys. Rev. Lett.* **127**, 261802 (2021), [arXiv:2107.13438 \[hep-ex\]](https://arxiv.org/abs/2107.13438).

[4] P. Agnes *et al.* (DarkSide-50), “Search for low-mass dark matter WIMPs with 12 ton-day exposure of DarkSide-50,” *Phys. Rev. D* **107**, 063001 (2023), [arXiv:2207.11966 \[hep-ex\]](https://arxiv.org/abs/2207.11966).

[5] Prakruth Adari *et al.* (SENSEI), “First Direct-Detection Results on Sub-GeV Dark Matter Using the SENSEI Detector at SNOLAB,” *Phys. Rev. Lett.* **134**, 011804 (2025), [arXiv:2312.13342 \[astro-ph.CO\]](https://arxiv.org/abs/2312.13342).

[6] J. Aalbers *et al.* (LZ), “Dark Matter Search Results from 4.2 Tonne-Years of Exposure of the LUX-ZEPLIN (LZ) Experiment,” *Phys. Rev. Lett.* **135**, 011802 (2025), [arXiv:2410.17036 \[hep-ex\]](https://arxiv.org/abs/2410.17036).

[7] G. Angloher *et al.* (CRESST), “First observation of single photons in a CRESST detector and new dark matter exclusion limits,” *Phys. Rev. D* **110**, 083038 (2024), [arXiv:2405.06527 \[astro-ph.CO\]](https://arxiv.org/abs/2405.06527).

[8] E. Aprile *et al.* (XENON), “WIMP Dark Matter Search using a 3.1 tonne \times year Exposure of the XENONnT Experiment,” (2025), [arXiv:2502.18005 \[hep-ex\]](https://arxiv.org/abs/2502.18005).

[9] C. Boehm and Pierre Fayet, “Scalar dark matter candi-

dates,” *Nucl. Phys. B* **683**, 219–263 (2004), arXiv:hep-ph/0305261.

[10] Dan Hooper and Kathryn M. Zurek, “A Natural Supersymmetric Model with MeV Dark Matter,” *Phys. Rev. D* **77**, 087302 (2008), arXiv:0801.3686 [hep-ph].

[11] Jonathan L. Feng and Jason Kumar, “The WIMPless Miracle: Dark-Matter Particles without Weak-Scale Masses or Weak Interactions,” *Phys. Rev. Lett.* **101**, 231301 (2008), arXiv:0803.4196 [hep-ph].

[12] Adam Falkowski, Joshua T. Ruderman, and Tomer Volansky, “Asymmetric Dark Matter from Leptogenesis,” *JHEP* **05**, 106 (2011), arXiv:1101.4936 [hep-ph].

[13] Yonit Hochberg, Eric Kuflik, Tomer Volansky, and Jay G. Wacker, “Mechanism for Thermal Relic Dark Matter of Strongly Interacting Massive Particles,” *Phys. Rev. Lett.* **113**, 171301 (2014), arXiv:1402.5143 [hep-ph].

[14] Raffaele Tito D’Agnolo and Joshua T. Ruderman, “Light Dark Matter from Forbidden Channels,” *Phys. Rev. Lett.* **115**, 061301 (2015), arXiv:1505.07107 [hep-ph].

[15] Eric Kuflik, Maxim Perelstein, Nicolas Rey-Le Lorier, and Yu-Dai Tsai, “Elastically Decoupling Dark Matter,” *Phys. Rev. Lett.* **116**, 221302 (2016), arXiv:1512.04545 [hep-ph].

[16] Raffaele Tito D’Agnolo, Cristina Mondino, Joshua T. Ruderman, and Po-Jen Wang, “Exponentially Light Dark Matter from Coannihilation,” *JHEP* **08**, 079 (2018), arXiv:1803.02901 [hep-ph].

[17] Rouven Essig, Jeremy Mardon, and Tomer Volansky, “Direct Detection of Sub-GeV Dark Matter,” *Phys. Rev. D* **85**, 076007 (2012), arXiv:1108.5383 [hep-ph].

[18] Chris Kouvaris and Josef Pradler, “Probing sub-GeV Dark Matter with conventional detectors,” *Phys. Rev. Lett.* **118**, 031803 (2017), arXiv:1607.01789 [hep-ph].

[19] M. F. Albakry *et al.* (SuperCDMS), “A Strategy for Low-Mass Dark Matter Searches with Cryogenic Detectors in the SuperCDMS SNOLAB Facility,” in *Snowmass 2021* (2022) arXiv:2203.08463 [physics.ins-det].

[20] I. Colantoni *et al.*, “BULLKID: BULKy and Low-Threshold Kinetic Inductance Detectors,” *J. Low Temp. Phys.* **199**, 593–597 (2020).

[21] Belina von Krosigk *et al.*, “DELight: A Direct search Experiment for Light dark matter with superfluid helium,” *SciPost Phys. Proc.* **12**, 016 (2023), arXiv:2209.10950 [hep-ex].

[22] Sinéad M. Griffin, Guy Daniel Hadas, Yonit Hochberg, Katherine Inzani, and Benjamin V. Lehmann, “Dark-Matter–Electron Detectors for Dark-Matter–Nucleon Interactions,” *Phys. Rev. Lett.* **135**, 141803 (2025), arXiv:2412.16283 [hep-ph].

[23] G. Angloher *et al.*, “The CRESST experiment: towards the next-generation of sub-GeV direct dark matter detection,” (2025), arXiv:2505.01183 [astro-ph.CO].

[24] T. K. Bui *et al.* (TESSERACT), “First Limits on Light Dark Matter Interactions in a Low Threshold Two-Channel Athermal Phonon Detector from the TESSERACT Collaboration,” *Phys. Rev. Lett.* **135**, 161002 (2025), arXiv:2503.03683 [hep-ex].

[25] A. Bento *et al.*, “The SWEET project: probing sugar crystals for direct dark matter searches,” (2025), arXiv:2510.00068 [physics.ins-det].

[26] E. Aprile *et al.* (XENON), “Search for Light Dark Matter Interactions Enhanced by the Migdal Effect or Bremsstrahlung in XENON1T,” *Phys. Rev. Lett.* **123**, 241803 (2019), arXiv:1907.12771 [hep-ex].

[27] P. Agnes *et al.* (DarkSide), “Search for Dark-Matter–Nucleon Interactions via Migdal Effect with DarkSide-50,” *Phys. Rev. Lett.* **130**, 101001 (2023), arXiv:2207.11967 [hep-ex].

[28] Di Huang *et al.* (PandaX Collaboration), “Search for dark-matter–nucleon interactions with a dark mediator in pandaX-4t,” *Phys. Rev. Lett.* **131**, 191002 (2023).

[29] A. Apponi *et al.* (PTOLEMY), “Heisenberg’s uncertainty principle in the PTOLEMY project: A theory update,” *Phys. Rev. D* **106**, 053002 (2022), arXiv:2203.11228 [hep-ph].

[30] Francesco Delfino, Carles Ros, Sidney M. Palardonio, Nina M. Carretero, Sebastián Murcia-López, Juan Ramón Morante, Jordi Martorell, Zacharias G. Fthenakis, Mauro Francesco Sgroi, Valentina Tozzini, *et al.*, “Multi-methodological analysis of hydrogen desorption from graphene,” *Carbon* **227**, 119211 (2024).

[31] Andrea Casale, Angelo Esposito, Guido Menichetti, and Valentina Tozzini, “The β -decay spectrum of Tritiated graphene: combining nuclear quantum mechanics with Density Functional Theory,” (2025), arXiv:2504.13259 [hep-ph].

[32] G. Cavoto, F. Luchetta, and A. D. Polosa, “Sub-GeV Dark Matter Detection with Electron Recoils in Carbon Nanotubes,” *Phys. Lett. B* **776**, 338–344 (2018), arXiv:1706.02487 [hep-ph].

[33] Yonit Hochberg, Yonatan Kahn, Mariangela Lisanti, Christopher G. Tully, and Kathryn M. Zurek, “Directional detection of dark matter with two-dimensional targets,” *Phys. Lett. B* **772**, 239–246 (2017), arXiv:1606.08849 [hep-ph].

[34] F. Pandolfi, A. Apponi, G. Cavoto, C. Mariani, I. Rago, and A. Ruocco, “The dark-PMT: a novel directional light Dark Matter detector based on vertically-aligned carbon nanotubes,” *J. Phys. Conf. Ser.* **2156**, 012051 (2021).

[35] Riccardo Catena, Timon Emken, Marek Matas, Nicola A. Spaldin, and Einar Urdshals, “Direct searches for general dark matter-electron interactions with graphene detectors: Part II. Sensitivity studies,” *Phys. Rev. Res.* **5**, 043258 (2023), arXiv:2303.15509 [hep-ph].

[36] Riccardo Catena, Timon Emken, Marek Matas, Nicola A. Spaldin, and Einar Urdshals, “Direct searches for general dark matter-electron interactions with graphene detectors: Part I. Electronic structure calculations,” *Phys. Rev. Res.* **5**, 043257 (2023), arXiv:2303.15497 [hep-ph].

[37] M. G. Betti *et al.* (PTOLEMY), “Neutrino physics with the PTOLEMY project: active neutrino properties and the light sterile case,” *JCAP* **07**, 047 (2019), arXiv:1902.05508 [astro-ph.CO].

[38] Mahmoud Mohamed Saad Abdelnabi, Chiara Izzo, Elena Blundo, Maria Grazia Betti, Marco Sbroscia, Giulia Di Bella, Gianluca Cavoto, Antonio Polimeni, Isabel García-Cortés, Isabel Rucandio, *et al.*, “Deuterium adsorption on free-standing graphene,” *Nanomaterials* **11**, 130 (2021).

[39] Maria Grazia Betti, Ernesto Placidi, Chiara Izzo, Elena Blundo, Antonio Polimeni, Marco Sbroscia, José Avila, Pavel Dudin, Kailong Hu, Yoshikazu Ito, *et al.*, “Gap opening in double-sided highly hydrogenated free-standing graphene,” *Nano letters* **22**, 2971–2977 (2022).

[40] Sammar Tayyab, Alice Apponi, Maria Grazia Betti, Elena Blundo, Gianluca Cavoto, Riccardo Frisenda, Nuria Jiménez-Arévalo, Carlo Mariani, Francesco Pandolfi, Antonio Polimeni, *et al.*, “Spectromicroscopy study of in-

duced defects in ion-bombarded highly aligned carbon nanotubes,” *Nanomaterials* **14**, 77 (2023).

[41] Alice Apponi, Orlando Castellano, Daniele Paoloni, Domenica Convertino, Neeraj Mishra, Camilla Coletti, Carlo Mariani, and Alessandro Ruocco, “Highly hydrogenated monolayer graphene with wide band gap opening,” (2025), arXiv:2504.10238 [cond-mat.mtrl-sci].

[42] Alice Apponi *et al.*, “Stability of highly hydrogenated monolayer graphene in ultra-high vacuum and in air,” *Appl. Surf. Sci.* **723**, 165658 (2026), arXiv:2504.11853 [cond-mat.mtrl-sci].

[43] Alice Apponi *et al.*, “Stability of Highly Hydrogenated Monolayer Graphene in Ultra-High Vacuum and in Air,” (2025), arXiv:2504.11853 [cond-mat.mtrl-sci].

[44] M. Simson, P. Holl, A.R. Müller, A. Niculae, G. Petzoldt, K. Schreckenbach, H. Soltau, L. Strüder, H.-F. Wirth, and O. Zimmer, “Detection of low-energy protons using a silicon drift detector,” *Nuclear Instruments and Methods in Physics Research Section A: Accelerators, Spectrometers, Detectors and Associated Equipment* **581**, 772–775 (2007).

[45] Walter Kohn and Lu Jeu Sham, “Self-consistent equations including exchange and correlation effects,” *Physical review* **140**, A1133 (1965).

[46] Feliciano Giustino, *Materials modelling using density functional theory: properties and predictions* (Oxford University Press, 2014).

[47] Mukul Kumar and Yoshinori Ando, “Chemical vapor deposition of carbon nanotubes: a review on growth mechanism and mass production,” *Journal of nanoscience and nanotechnology* **10**, 3739–3758 (2010).

[48] Yabin Chen and Jin Zhang, “Chemical vapor deposition growth of single-walled carbon nanotubes with controlled structures for nanodevice applications,” *Accounts of chemical research* **47**, 2273–2281 (2014).

[49] Til Piffl *et al.*, “The RAVE survey: the Galactic escape speed and the mass of the Milky Way,” *Astron. Astrophys.* **562**, A91 (2014), arXiv:1309.4293 [astro-ph.GA].

[50] G. Monari, B. Famaey, I. Carrillo, T. Piffl, M. Steinmetz, R. F. G. Wyse, F. Anders, C. Chiappini, and K. Janßen, “The escape speed curve of the Galaxy obtained from Gaia DR2 implies a heavy Milky Way,” *Astron. Astrophys.* **616**, L9 (2018), arXiv:1807.04565 [astro-ph.GA].

[51] Xiaowei Ou, Anna-Christina Eilers, Lina Necib, and Anna Frebel, “The dark matter profile of the milky way inferred from its circular velocity curve,” *Monthly Notices of the Royal Astronomical Society* **528**, 693–710 (2024).

[52] L. M. Capparelli, G. Cavoto, D. Mazzilli, and A. D. Polosa, “Directional Dark Matter Searches with Carbon Nanotubes,” *Phys. Dark Univ.* **9-10**, 24–30 (2015), [Erratum: *Phys. Dark Univ.* 11, 79–80 (2016)], arXiv:1412.8213 [physics.ins-det].

[53] G. Cavoto, E. N. M. Cirillo, F. Cocina, J. Ferretti, and A. D. Polosa, “WIMP detection and slow ion dynamics in carbon nanotube arrays,” *Eur. Phys. J. C* **76**, 349 (2016), arXiv:1602.03216 [physics.ins-det].

[54] S. Hu, M. Lozada-Hidalgo, F. C. Wang, Artem Mishchenko, F. Schedin, E. W. Nair, Rahul Raveendran andgHill, D. W. Boukhvalov, M. I. Katsnelson, Robert A. W. Dryfe, *et al.*, “Proton transport through one-atom-thick crystals,” *Nature* **516**, 227–230 (2014).

[55] Marcelo Lozada-Hidalgo, Sheng Zhang, Sheng Hu, Vasily G. Kravets, Francisco J. Rodriguez, Alexey Berdyugin, Alexander Grigorenko, and Andre K. Geim, “Giant photoeffect in proton transport through graphene membranes,” *Nature nanotechnology* **13**, 300–303 (2018).

[56] Eoin Griffin, Lucas Mogg, Guang-Ping Hao, Gopinadhan Kalon, Cihan Bacaksiz, Guillermo Lopez-Polin, T. Y. Zhou, Victor Guarachico, Junhao Cai, Christof Neumann, *et al.*, “Proton and li-ion permeation through graphene with eight-atom-ring defects,” *Acs Nano* **14**, 7280–7286 (2020).

[57] Zhiyang Zeng, Ruiyang Song, Shengping Zhang, Xiao Han, Zhen Zhu, Xiaobo Chen, and Luda Wang, “Biomimetic n-doped graphene membrane for proton exchange membranes,” *Nano Letters* **21**, 4314–4319 (2021).

[58] Oluwasegun J Wahab, E. Daviddi, B. Xin, P. Z. Sun, E. Griffin, A. W. Colburn, D. Barry, M. Yagmurcukardes, F. M. Peeters, A. K. Geim, *et al.*, “Proton transport through nanoscale corrugations in two-dimensional crystals,” *Nature* **620**, 782–786 (2023).

[59] Jincheng Tong, Yangming Fu, Daniil Domaretskiy, F. Della Pia, Parveen Dagar, Lewis Powell, D. Bahamont, Shiqi Huang, Benhao Xin, R. N. Costa Filho, *et al.*, “Control of proton transport and hydrogenation in double-gated graphene,” *Nature* **630**, 619–624 (2024).

[60] S. Horiguchi, K. Koyama, and Y. H. Ohtsuki, “Auger neutralization of slow protons at solid surfaces,” *physica status solidi (b)* **87**, 757–763 (1978).

[61] H. Winter, R. Kirsch, J. C. Poizat, and J. Remillieux, “Neutralization of fast protons in grazing collisions with a clean al(111) surface,” *Phys. Rev. A* **43**, 1660–1662 (1991).

[62] H. Jouin and F. A. Gutierrez, “Velocity dependence of outgoing neutral fractions for h(1s) and h⁺ beams impinging on al(111) at grazing incidence,” *Phys. Rev. A* **84**, 014901 (2011).

[63] R. Zimny, Z. L. Mišković, N. N. Nedeljković, and Lj. D. Nedeljković, “Interplay of resonant and auger processes in proton neutralization after grazing surface scattering,” *Surface Science* **255**, 135–156 (1991).

[64] Luca Cecchini, Carlo Pepe, Benedetta Corcione, Orlando Castellano, Daniele Paoloni, Federico Malnati, Gianluca Cavoto, Marco Carminati, Carlo Fiorini, Giorgio Pettinari, Ravi Prakash Yadav, Ilaria Rago, Alice Apponi, Andrei Puiu, Carlo Mariani, Mauro Rajteri, Alessandro Ruocco, and Francesco Pandolfi, “Quantitative correlation between carbon nanotube tip morphology and field emission properties at cryogenic temperature,” *Nanoscale* **17**, 21260–21267 (2025).

[65] S. Baroni, S. de Gironcoli, A. Dal Corso, and P. Giannozzi, “Phonons and related crystal properties from density-functional perturbation theory,” *Rev Mod Phys* **73**, 515–562 (2001).

[66] Arkadii B. Migdal, *Qualitative Methods in Quantum Theory*, Frontiers in Physics, Vol. 48 (W. A. Benjamin, Inc. (Advanced Book Program), Reading, MA, 1977).

[67] Ravishankar Sundararaman, Kendra Letchworth-Weaver, Kathleen A. Schwarz, Deniz Gunceler, Yalcin Ozhabes, and Tomás A. Arias, “Jdftx: Software for joint density-functional theory,” *SoftwareX* **6**, 278–284 (2017).

[68] John P. Perdew, Kieron Burke, and Matthias Ernzerhof, “Generalized gradient approximation made simple,” *Phys. Rev. Lett.* **77**, 3865–3868 (1996).

[69] Martin Schlipf and François Gygi, “Optimization algorithm for the generation of oncv pseudopotentials,” *Computer Physics Communications* **196**, 36–44 (2015).

[70] Ravishankar Sundararaman and T. A. Arias, “Regular-

ization of the coulomb singularity in exact exchange by wigner-seitz truncated interactions: Towards chemical accuracy in nontrivial systems,” *Phys. Rev. B* **87**, 165122 (2013).

[71] Richard M. Martin, *Electronic Structure: Basic Theory and Practical Methods* (Cambridge University Press, 2004).